Published in final edited form as:
J Mater Chem A Mater Energy Sustain. 2013 February 7; 1(5): 1557–1565. doi:10.1039/C2TA00415A.

Controlling Morphology and Molecular Packing of Alkane Substituted Phthalocyanine Blend Bulk Heterojunction Solar Cells†

Matthew J. Jurow[a], **Brian A. Hageman**[a], **Elaine DiMasi**[b], **Chang-Yong Nam**[c], **Cesar Pabon**[a], **Charles T. Black**[c], and **Charles Michael Drain**[a,d]

Elaine DiMasi: DiMasi@bnl.gov; Charles Michael Drain: Cdrain@hunter.cuny.edu

[a]Department of Chemistry, Hunter College of The City University of New York, New York, New York 10065

[b]Photon Sciences Division BLDG 728M, Brookhaven National Laboratory, Upton, New York 11973

[c]Center for Functional Nanomaterials, Brookhaven National Laboratory, Upton, New York 11973

[d]The Rockefeller University, New York, New York 10065

Abstract

Systematic changes in the exocyclic substiution of core phthalocyanine platform tune the absorption properties to yield commercially viable dyes that function as the primary light absorbers in organic bulk heterojunction solar cells. Blends of these complementary phthalocyanines absorb a broader portion of the solar spectrum compared to a single dye, thereby increasing solar cell performance. We correlate grazing incidence small angle x-ray scattering structural data with solar cell performance to elucidate the role of nanomorphology of active layers composed of blends of phthalocyanines and a fullerene derivative. A highly reproducible device architecture is used to assure accuracy and is relevant to films for solar windows in urban settings. We demonstrate that the number and structure of the exocyclic motifs dictate phase formation, hierarchical organization, and nanostructure, thus can be employed to tailor active layer morphology to enhance exciton dissociation and charge collection efficiencies in the photovoltaic devices. These studies reveal that disordered films make better solar cells, short alkanes increase the optical density of the active layer, and branched alkanes inhibit unproductive homogeneous molecular alignment.

Introduction

Semi-transparent organic photovoltaic (OPV) devices have applications as functional window coatings in urban settings where the surface area is greater on the sides of buildings than the roofs, but have reduced efficiencies *a prori* because of the reduced optical density of the active layer.[1-5] OPV devices have drawn tremendous research interest for their potential cost-effectiveness, lightweight flexible device form factors, and readily available components with low toxicity.[1, 2, 6-13] Many state-of-the-art OPV devices use a bulk

†Electronic Supplementary Information (ESI) available: Synthesis and characterization of the ZnPc dyes, AFM of the film thicknesses, UV-visible spectra of the films and typical GISAX data, band gaps and HOMO-LUMO gaps of some of the ZnPc dyes, IPCE compared to the absorbance of a ZnPc-C12 blend cell.

Correspondence to: Elaine DiMasi, DiMasi@bnl.gov; Charles Michael Drain, Cdrain@hunter.cuny.edu.

heterojunction (BHJ) architecture, wherein an interpenetrating network of donor and acceptor materials are in contact with an anode and a cathode.[10, 14-16] In BHJ, a phase separated bicontinuous donor-acceptor network with optimized inter-domain distances and interfacial areas maximize exciton dissociation into free charge carriers and minimize charge recombination.[6, 17] Thus, the nanomorphology of the active layer is a key factor dictating device performance.[18-21] Small organic dye molecules show significant potential as efficient donor components in OPV devices.[10, 22-25] Phthalocyanines (Pc) are tetra-isoindole macrocycles with absorptivity of $>10^5$ in the red region of the solar spectrum and photonic properties that enable materials for OPV devices;[25, 26] e.g. copper Pc,[27] and a zinc Pc with a C_{60} derivative in conducting polymers in the heterojunction.[28-32] We previously demonstrated that the HOMO-LUMO gap of Pc can be controlled by the number and electronic properties of substituents on the periphery of a core Pc platform[33] thereby tuning the lowest energy Q absorption band λ_{max} from *ca.* 650 nm to *ca.* 750 nm where there is a high flux of solar photons.[34-36]

As part of an effort to develop semi-transparent OPV films for urban applications, we also demonstrated that a blend of these commercially viable Pc with complimentary absorption bands produces an active layer in a BHJ device that covers a broader swath of the solar spectrum, and results in substantial improvements in efficiency over cells made of only one Pc.[33] Other blended devices, including some with fullerenes, display improvements in short circuit current densities.[12, 17, 37] The organization of the active layers of BHJ devices,[38] evaporated CuPc on glass,[39] and other device designs[40-42] were evaluated by x-ray methods. The present work uses grazing incidence small angle x-ray scattering (GISAXS) to investigate the relationships between photovoltaic (PV) performance and the hierarchical self-organization[43-46] of the active layer in solution processed BHJ devices as controlled by the structures of the Pc.

Herein, devices are produced from a blended solution of commercially viable Pc dyes with absorption bands in the 600-800 nm range and a functionalized fullerene electron acceptor incorporated into a simple and robust film that serves as a model for OPV coatings. The performance of these devices is on par with current state-of-the-art Pc-based OPV.[24] Using thioalkanes with different chemical structures (Figure 1) produces a family of molecules that are chemically compatible but yield nanofilms with marked morphological differences. We avoided established strategies that increase OPV efficiency but compromise commercial viability and/or reproducibility such as covalent linking of dyes,[47] layering by thermal evaporation to create more panchromatic devices,[48, 49] and cell architectures that are difficult to fabricate and quantitatively reproduce.[22, 50-52] Other strategies that affect active layer morphology have been studied.[17, 53, 54]

To correlate the changes in nanomorphology of the active layer to device performance, we have selected a simplified BHJ type solar cell architecture (Figure 2) which is easily fabricated in open air and easily reproduced in different laboratories without requiring the complex organic photovoltaic (OPV) architectures necessary for greater efficiencies.[55-58] This architecture allows GISAXS studies to be correlated with higher precision device characterization. Herein we demonstrate several key factors that improve device efficiency: (a) short side chains on the PC increased the active layer optical density, (b) increasing disorder in the films diminished domain size, and (c) diminishing the homogeneous alignment decreased non-productive charge dislocation.

Materials and Methods

All solvents and reagents were purchased from Sigma-Aldrich and used without further purification unless otherwise stated. Fullerene C_{60} (99.5%) was obtained from BuckyUSA.

A Cary Bio-1 was used for UV-visible spectra, and an Asylum (MFP-3D, Asylum Research Corp.) was used for atomic force microscopy (AFM) measurements. All syntheses, device fabrications, and device measurements were performed multiple times by different researchers.

All device samples (Figure 2) were prepared by first spin coating a PEDOT:PSS hole conducting layer, in open air, approximately 55 nm thick onto a pre-cleaned 140 nm thick indium tin oxide (ITO) coated glass substrate at 5,000 RPM from aqueous solution and baked at 140 °C for 10 minutes. An active layer was deposited by spin coating at 700 RPM for 45 seconds from toluene solutions of either an individual Pc derivative at 0.5% (w/w) (Pc-4-C5, Pc-8-C5, Pc-4-C8, Pc-8-C8, Pc-4-C12, Pc-8-C12, see Figure 1 and Table 1) or a blend of a four substituted, eight substituted, and *tert*-butyl Pc at relative ratios of 17:66:17 (w/w) at a total concentration of 0.25% (w/w) (Pc-C5 blend, Pc-C8 blend, Pc-C12 blend) to form a 75 nm thick film as measured by AFM. In all cases the Pc were mixed with 30% (w/w) of a pyridyl fullerene (PyC_{60})[59, 60] (w/w) relative to the total dye content. These samples were investigated by grazing-incidence x-ray diffraction. For PV device characterization, ~40 nm thick fullerene (C_{60}) and 70 nm thick aluminium top contacts were sequentially deposited through a shadow mask (active device area: 3.14 mm^2) in vacuum by thermal evaporation on top of the active blend layer (Figure 2). Device performance parameters were measured in open air.

Synchrotron x-ray scattering measurements were made at the National Synchrotron Light Source. Data was collected at Beamline X6B using a Princeton Instruments CCD area detector and at Beamline X9A with a MARCCD detector. At X6B, measurements were made with an adjustable sample-detector distance of 16 to 50 cm, at wavelengths ranging from 0.65 Å to 1.2 Å to survey possible order on length scales from 3 Å to 40 Å. First-order diffraction peaks with d-spacings approximately 25-35 Å were the only ones detected for all samples. Incidence angles of 0.07, 0.12 and 0.20 degrees were compared, and peak to background ratios found to be similar. All X6B data shown have the following configuration: detector distance 16 cm, wavelength 1.215 Å, and incident angle 0.12 degrees. At Beamline X9A measurements were made at a detector distance of 24.9 cm (+/− 2mm) at a wavelength of 0.89 Å providing an accessible q-range from 0.13-2.89 $Å^{-1}$ corresponding to a length range of *ca.* 2-50 Å. Images taken using the X6B and X9A Beamlines were calibrated using powder standards (alumina and/or silver behenate) and analyzed using Datasqueeze [http://datasqueezesoftware.com] to integrate and plot the scattered x-ray intensity versus momentum transfer q and azimuthal angle χ around the incident beam direction. Fits from collected data sets were evaluated using FitYK [http://fityk.nieto.pl/]. Gaussian line shapes were used to quantify the peaks and extract full width at half maximum (FWHM) values.

PV parameters of fabricated devices were measured from device current-voltage (I-V) characteristics under simulated solar illumination. A custom-modified probe station equipped with Agilent 4156C precision semiconductor parameter analyzer was used to characterize dark and illuminated I-V characteristics, and an Oriel 9600 150 W solar simulator with an AM1.5G filter was used for solar illumination with 100 mW/cm^2 (1 SUN) condition (calibrated by Oriel 70268 thermopile detector).

All dyes were synthesized by similar procedures with minor modifications to yield a library of Pc having various degrees of peripheral thioalkane substitution, with tuned optical properties (Table 1).[33] All molecules, except for the tetra-*tert*-butyl Pc (ZnPc-4-TBu) which was purchased from Aldrich and used as received, were fabricated from the same starting material, zinc 1,2,3,4,8,9,10,11,15,16,17,18,22,23,24,25-hexadeca-fluoro-phthalocyaninato zinc(II), ($ZnPcF_{16}$), also obtained from Sigma.

Device Architecture

The device architecture is depicted in Figure 2. Active layers were spin cast from toluene solutions of either a single Pc, or a blend of multiple Pc, and a pyridyl functionalized fullerene acceptor, PyC_{60}. Contacts were then thermally evaporated. The degree of substitution of the phthalocyanine is controlled by variation of reaction conditions: temperature, duration, and solvent (see supporting information). The UV-visible absorption spectrum allows for easy tracking of the degree of peripheral substitution on the core $ZnPcF_{16}$ platform by following the *ca.* 7 nm red shift of the strongly absorptive Q bands for each electron withdrawing fluorine substituted by an electron donating thioalkane.[33, 34] The substitution occurs initially at the more reactive β positions of the starting $ZnPcF_{16}$ (Figure 1), which has a strong absorption at 680 nm. Derivatives with one or two thioalkanes on the β positions of each isoindole have optical bands centered at 707 nm and 735 nm, respectively (Table 1). The acceptor, PyC_{60}, was synthesized according to literature procedures.[59]

We focus on readily available, cost effective, and scalable materials that can be incorporated into simple devices with easily reproducible efficiencies. The layers are spin coated in ambient atmosphere from non-halogenated solvents to produce a stable device from which we can assess the effect of variations in active layer composition and nanomorphologies. The active layer contains a blend of one or more Pc dye donors and PyC_{60}, which serves as an electron acceptor. The pyridyl moiety on the PyC_{60} acceptor can coordinate to the Zn(II) center of the Pc molecules to facilitate charge transfer and exciton diffusion at the donor-acceptor interface.[61, 62] Though modifications of the fullerene diminish its effectiveness as an electron acceptor, neither unfunctionalized C_{60} or the commonly used phenyl-C_{61}-butyric-acid-methyl ester (PCBM) work well in this device architecture because C_{60} is not adequately soluble at the necessary concentration and PCBM creates poor quality cells that phase separate upon annealing.

The facile chemistry on the $ZnPcF_{16}$ allows tuning of the UV-visible spectra and formation of chemically compatible and photonically complementary dyes with significant overlap of the HOMO-LUMO gaps. Thus, a blend of these Pc dyes effectively uses a greater part of the solar spectrum as evidenced by EQE measurements in our previous work (see supporting information).[33] The use of different thioalkanes preserves these chemical similarities and the advantages of blending multiple dyes while allowing for controlled variation of hierarchical organization and optical density (Figure 3). The shorter chains form films with greater optical density because the alkanes occupy less surface area in the active layer and allow for a higher packing density of the Pc cores.

Hydrocarbon Structure Dictates Hierarchical Order and Device Efficiency

Power conversion efficiencies depend on thioalkane chain length (Figure 4, Table 2). We hypothesized that the use of the ZnPc-C12 Blend within the active layer displayed low overall device power conversion efficiencies (PCE) due in part to the resistivity of the device's active layer. In order to decrease the device resistance and simultaneously improve optical density by packing more chromophores into the same thickness of the cast layer, devices using ZnPc-C5 with short pentanethiol chains were evaluated. Devices made with a ZnPc-C5 blend exhibited nearly a 100% increase in PCE compared with devices containing the ZnPc-C12 blend, due in large part to a 60% increase in J_{SC}, a 25% increase in V_{OC}, and a ~40% decrease in device series resistance as determined from the tangential slope at $V_{OC.}$ Devices with only ZnPc-4-C5 in the active layer displayed nearly identical R_S but 20% lower PCE because of reduced V_{OC} and J_{SC} compared to devices with the ZnPc-C5 blend. Thus for a given ZnPc core system, the thioalkane length is the main factor that determines

device R_S rather than the number of attached thioalkanes. As discussed below, the dependence of R_S on the length of side thioalkane chain suggests that the molecular stacking of Pc occurs parallel to the film plane.

Liquid Crystalline Domains

Pc have disk shaped structures that are about 1.5 nm in diameter and can form discotic liquid crystal phases (DLC) when appended with long-chain alkanes.[63-67] DLC can be induced to arrange themselves into columns stacked parallel to the substrate (homogeneous alignment) or perpendicular to the substrate (homeotropic alignment) as illustrated in Figure 5. DLC exhibit excellent electron transfer along the columnar axis and are used in a variety of widely deployed technologies such as LCD screens and OPV.[63, 68, 69] A film of homeotropically aligned, co-facially pi stacked Pc would be expected to rapidly transmit charge perpendicularly to the substrate and could be expected to approach the ideal bulk heterojunction architecture.[2, 70-72]

In the case of a homogeneously aligned film, x-ray scattering measurements with the incident beam grazing the film surface exhibit hexagonal scattering patterns for well aligned films. For intermolecular spacing a (on the order of the molecular disk diameter), the spacing of diffracting planes $d = a(\sqrt{3}/2)$, yields diffraction spots with momentum transfer $q = 2\pi/d$, which is analyzed from the radial position of the diffracted beam. The six-fold symmetry creates three spots above the film horizon, as shown in the diffraction pattern of Pc-8-C12 (Figure 5c). The additional streak of intensity along the vertical axis arises from x-rays reflecting from the smooth film surface, and the dark shadows are from the beam stop. The magnitude of q and the width of the peak along q indicate the d-spacing and the distribution of d-spacings of the molecular columns.

The azimuthal angle χ provides information about film alignment. Figure 5d shows a graph of diffracted intensity, integrated over a small q interval at the diffracted peaks. The maxima at 30°, 90°, and 150° confirm hexagonal symmetry and homogeneous alignment for Pc-8-C12. The peak width in χ directly probes the orientations of the ordered grains. For example, small domains may be present whose hexagonal stacks do not lie parallel to the substrate, as depicted in Figure 5e. A distribution of crystalline regions will broaden the peaks along the χ direction. If the collection of grains has isotropic orientation, a diffraction ring with intensity independent of χ will be observed.

A range in q was surveyed to enable d-spacings from 3 Å to 40 Å to be detected for all samples. No wide-angle peaks were observed, indicating insufficient diffraction contrast from long-range-ordered columnar pi-stacking of the molecules in any orientation. Instead, diffraction peaks were observed for columnar structures with hexagonal symmetry evident only in the detector plane. Thus, all diffracting dye molecules are oriented homogenously (Figure 5b, 5e).

Diffraction peaks were observed with q maxima ranging from 0.23 $Å^{-1}$ to 0.33 $Å^{-1}$, corresponding to column layer spacings of 19 Å to 27 Å, or inter-column distances of 22 Å to 31.5 Å, as expected for their molecular diameters with extended hydrocarbon chains of varying length. For active layer films, the diffraction peaks exhibited variations in widths of both q and χ among samples, and were never resolved into contributions from multiple peaks. This observation suggests that the samples, including the blends, consist of no more than one LC phase. In samples displaying the most order, sharp spots are observed at the expected azimuthal angles indicative of a hexagonally packed homogeneously aligned film.[73] The peak corresponds to the (1,1) hexagonal column and indicates a center-to-center distance of 30.9 Å for the C_{12} film that is consistent with the molecular diameter of 25-35 Å with extended side chains.

Improving Device Performance by Frustrating Homogenous Order

Our previously work with the ZnPc-C12 Blend system demonstrated that the inclusion of a small percentage of ZnPc-4-TBu into a Pc mixture resulted in an increase in PCE which far exceeded the gain expected solely from the increased spectral coverage.[33] Because of the impact active layer nanostructure has on the photonic properties of these films, GISAXS measurements were made on devices to examine the effects of both the incorporation of the ZnPc-4-TBu and the inclusion of dyes with different thioalkane side chains.

Films of ZnPc-8-C12 and ZnPc-4-C12 with PyC_{60} were found to exhibit homogeneous packing, with diffraction patterns similar to that shown in figure 5c (compare Figures 6 and 7). This observation is consistent with Pc molecules bearing long hydrocarbon chains stacking into liquid crystalline phases.[63-65, 74-76] Charge transport in the normal direction in films with homogeneous alignment (Figure 5b) is intrinsically inhibited by charge hopping across insulating side chains. Since the efficiency of inter-column charge hopping depends on the distance between macrocycle edges, the improved efficiencies observed in devices made from films containing domains of homogeneously aligned ZnPc-C5 arise from the shorter inter-column distances in addition to the increased optical cross sections.

The ZnPc-C8 dyes with branched thioalkanes improved theoptical cross section (Figure 3) relative to the Pc-C12 systems, but diminished the PV performance compared to the other devices. The absence of diffraction indicates a lack of uniformly ordered regions in the ZnPc-C8/PyC_{60} active layer, resulting in an increase of R_S by nearly twofold, and a ~35% decrease in J_{SC}, because of exciton recombination and poor charge collection.

Incorporating dyes with shorter alkyl chains increases the inter-domain conductivity between homogenously packed columns and also deters the formation of a homogenous mesophase. Blending with ZnPc-4-TBu diminishes homogenous LC order in the same fashion and results in increased device efficiency. X-ray data (Figure 7) indicates that Pc with fewer and shorter side chains form films with less of the unfavorable homogeneous ordering observed in the Pc-C12 dye systems. GISAXS data from both ZnPc-4-C5 and ZnPc-8-C5 films exhibit a diffuse halo, centered at q=0.31 $Å^{-1}$ (a=23 Å). With 5% (w/w) ZnPc-4-TBu in the ZnPc-4-C5 and ZnPc-8-C5 films, no diffraction patterns are observed, indicating a complete disruption of repeating regions of homogenous order.

The ZnPc-C8 films exhibited narrower q peak widths than those with ZnPc-C5, though still broader than the ZnPc-C12 films. Diffraction patterns for ZnPc-C8 suggest that the branched alkanes allow for somewhat better side chain melting, liquid crystallinity, and blending with acceptor than the C5 dye (Figure 6, 7). Both an increased degree of alkyl substitution and an increased chain length result in larger regions of homogeneously ordered molecules that negatively impacted PV efficiencies.

The homogeneous alignment of the Pc arises from the greater affinity of the appended alkanes for the PDOT:PSS surface than the macrocycle core.[77, 78] The lack of second order diffraction peaks implies that the domains of homogeneously packed molecules are small, likely because the 70 nm layers contain non- periodic interruptions in molecular arrangements caused by roughness in the PEDOT layer. Broadening of these peaks into halos and rings arises from a randomization in the orientation of the ordered regions. At wide scattering angles no other information, such as a d-spacing corresponding to a pi-stacking length, is observed.

Since blends of Pc can exhibit enhanced performance relative to the individual dyes, studies were done to discern whether the dye molecules segregated into domains or mixed well on a molecular level. The organization of a film of ZnPc-C12 blend was compared to films of the

individual C12 dyes alone. The GISAXS data from the blended films shows no clear evidence indicating the formation of domains composed of one of the dyes. The ZnPc-8-C12 film exhibits a bright, narrow diffraction peak, and the blends exhibit diffuse bands (Figure 6). This is consistent with earlier AFM friction studies and the notion that the dyes are chemically similar (Table 1).

The inclusion of 17% ZnPc-4-TBu into a mixture of ZnPc-4-C12 and ZnPc-8-C12 dyes increased the PCE by nearly 50%. A separate set of samples consisting of Pc-8-C12 blended with different ratios of ZnPc-4-TBu were prepared to quantify the effect of the latter on the morphology of the films and PCE. A blurred halo is observed in the GISAXS indicating the inclusion of the ZnPc-4-TBu disrupts the otherwise homogeneously ordered regions of the ZnPc-8-C12 in the film or reorients ordered sections of dyes into random directions (Figure 8). This induced disorder contributes substantially toward the improvement in solar cell efficiency in the blended devices relative to the cells composed solely of the individual dyes. Taken together, it is likely that the devices made from the individual dyes feature large regions of Pc molecules oriented parallel to the surface thereby inhibiting charge migration to the electrodes, and allowing rates of geminate and intermolecular charge recombination to compete with rates of exciton diffusion to a requisite interface. A small percentage of ZnPc-4-TBu is sufficient to frustrate homogeneous alignment.

The concept that long range homogenous order is detrimental to device efficiencies is also supported by the near elimination of any detectable PCE upon annealing. The multiple peaks at various q values as well as the diffuse halos observed in the diffraction images suggest that annealing induces substantial phase separation of the device components (Figure 9). AFM data collected of the annealed films after the collection of the x-ray images shows phase separated finger-like domains on the order of 100 nm high (Figure 9).

Conclusion

Blended dye systems have clear advantages.[29] Devices using dye blends made from a core Pc platform display remarkable improvement in photovoltaic efficiency of these semi-transparent functional coatings upon the integration of a small percentage of ZnPc-4-TBu because it disrupts the unfavorable homogenous packing of the dye molecules in the active layer.[79] The use of a core Pc platform also assures significant overlap of the HOMO-LUMO gaps of the dyes in the active layer, thereby facilitating charge transport.[33] Shorter side chain substituents such as ZnPc-C5 reduce both the film resistivity and the liquid crystalline character of the dyes, while increasing the optical density of the active layer. Many groups are investigating liquid crystalline molecules to serve as donors in organic bulk heterojunction solar cell devices.[63, 65, 74, 80] Homeotropically aligned systems of dyes with interdigitated domains of electron acceptors may be a good architecture for BHJ active layers;[1] however, difficulty in producing homeotropic packing remains an obstacle. The detrimental effect on cell performance resulting from the necessary alkyl substitution required to induce liquid crystallinity in Pc suggests that different methods of self-organization into favorable nanoarchitectures are needed. Understanding the effect of ZnPc-4-TBu in the ZnPc-C12 dye system, and the differences in nanostructure of films containing the three different thioalkane side chains, disorder may be a better design principle for devices with blended active layers. Further investigations will explore the effect of substitution with conducting side chains as well as their effect on morphology.

Supplementary Material

Refer to Web version on PubMed Central for supplementary material.

Acknowledgments

We thank Dr. R. Gearba and Dr. A. Varotto for assistance with experimental design, and Dr. L. Yang, Dr. K. Yager, and Dr. V. Stanic for assistance with the x-ray beam. We also thank Mr. J.Baris for helping to facilitate research, and N. P. Drain for the photos of the solar cells. This work was supported by the National Science Foundation (NSF, CHE- 0847997 and 0848602 to C.M.D.). Hunter College Science infrastructure is supported by the NSF, the National Institutes of Health (including the RCMI program RR003037 andMD007599), and CUNY. Research carried out at the Center for Functional Nanomaterials and the National Synchrotron Light Source at Brookhaven National Laboratory is supported under USDOE contract DE-AC02-98CH10886. This Research was carried out in part at the Center for Functional Nanomaterials, Brookhaven National Laboratory supported by the U.S. Department of Energy, Office of Basic Energy Sciences, under Contract No. DE-AC02-98CH10886.

Notes and references

1. Ameri T, Dennler G, Lungenschmied C, Brabec CJ. Energy Env Sci. 2009; 2:347–363.
2. Ratcliff EL, Zacher B, Armstrong NR. J Phys Chem Let. 2011; 2:1337–1350.
3. Liao KS, Yambem SD, Haldar A, Alley NJ, Curran SA. Energies. 2010; 3:1212–1250.
4. He F, Yu L. J Phys Chem Lett. 2011; 2:3102–3113.
5. Bailey-Salzman RF, Rand BP, Forrest SR. Appl Phys Lett. 2006; 88:233502–233503.
6. Clarke TM, Durrant JR. Chem Rev. 2010; 110:6736–6767. [PubMed: 20063869]
7. Liang Y, Yu L. Poly Rev. 2010; 50:454–473.
8. Zheng Y, Xue J. Poly Rev. 2010; 50:420–453.
9. Krebs FC, Fyenbo J, Tanenbaum DM, Gevorgyan SA, Andriessen R, van Remoortere B, Galagan Y, Jorgensen M. Energ Envir Sci. 2011; 4:4116–4123.
10. Walker B, Kim C, Nguyen TQ. Chem Mater. 2011; 23:470–482.
11. Ooyama Y, Harima Y. Eur J Org Chem. 2009; 2009:2903–2934.
12. Lee HJ, Leventis HC, Haque SA, Torres T, Grätzel M, Nazeeruddin MK. J Power Sources. 2011; 196:596–599.
13. Brabec CJ, Sariciftci NS, Hummelen JC. Adv Funct Mater. 2001; 11:15–26.
14. Peumans P, Uchida S, Forrest SR. Nature. 2003; 425:158–162. [PubMed: 12968174]
15. Scharber MC, Mühlbacher D, Koppe M, Denk P, Waldauf C, Heeger AJ, Brabec CJ. Adv Mat. 2006; 18:789–794.
16. Khan SM, Kaur M, Heflin JR, Sayyad MH. J Phys Chem Solids. 2011; 72:1430–1435.
17. Said AJ, Poize G, Martini C, Ferry D, Marine W, Giorgio S, Fages F, Hocq J, Bouclé J, Nelson J, Durrant JR, Ackermann J. J Phys Chem C. 2010; 114:11273–11278.
18. Sun Y, Welch GC, Leong WL, Takacs CJ, Bazan GC, Heeger AJ. Nat Mater. 2012; 11:44–48. [PubMed: 22057387]
19. Chu TY, Lu J, Beaupré S, Zhang Y, Pouliot JRm, Wakim S, Zhou J, Leclerc M, Li Z, Ding J, Tao Y. J Am Chem Soc. 2011; 133:4250–4253. [PubMed: 21375331]
20. Zhu Y, Xu X, Zhang L, Chen J, Cao Y. Solar Energy Materials Solar Cells. 2012; 97:83–88.
21. Jurow M, Schuckman AE, Batteas JD, Drain CM. Coord Chem Rev. 2010; 254:2297–2310. [PubMed: 20936084]
22. Loser S, Bruns CJ, Miyauchi H, Ortiz RoP, Facchetti A, Stupp SI, Marks TJ. J Am Chem Soc. 2011; 133:8142–8145. [PubMed: 21545133]
23. Lee CY, She C, Jeong NC, Hupp JT. Chem Commun. 2010; 46:6090–6092.
24. Ning Z, Fu Y, Tian H. Energy Environ Sci. 2010; 3:1170–1181.
25. Walter MG, Rudine AB, Wamser CC. J Porphyrins Phthalocyanines. 2010; 14:759–792.
26. de la Torre G, Claessens CG, Torres T. Chem Com. 2007:2000–2015.
27. Schumann S, Hatton RA, Jones TS. J Phys Chem C. 2011; 115:4916–4921.
28. D'Souza F, Ito O. Chem Soc Rev. 2012; 41:86–96. [PubMed: 21975532]
29. Honda S, Ohkita H, Benten H, Ito S. Adv Energy Mater. 2011; 1:588–598.
30. Zeng W, Yong KS, Kam ZM, Zhu F, Li Y. Appl Phys Let. 2010; 97:133304.
31. Honda S, Yokoya S, Ohkita H, Benten H, Ito S. J Phys Chem C. 2011; 115:11306–11317.

32. Honda S, Ohkita H, Benten H, Ito S. Chem Com. 2010; 46:6596–6598.
33. Varotto A, Nam CY, Radivojevic I, Tomé JPC, Cavaleiro JAS, Black CT, Drain CM. J Am Chem Soc. 2010; 132:2552–2554. [PubMed: 20136126]
34. Radivojevic I, Varotto A, Farley C, Drain CM. Energ Envir Sci. 2010; 3:1897–1909.
35. Blankenship RE, Tiede DM, Barber J, Brudvig GW, Fleming G, Ghirardi M, Gunner MR, Junge W, Kramer DM, Melis A, Moore TA, Moser CC, Nocera DG, Nozik AJ, Ort DR, Parson WW, RC Prince, Sayre RT. Science. 2011; 332:805–809. [PubMed: 21566184]
36. Rand BP, Genoe J, Heremans P, Poortmans J. Progress in Photovoltaics: Research and Applications. 2007; 15:659–676.
37. Moon SJ, Baranoff E, Zakeeruddin SM, Yeh CY, Diau WG, Gratzel M, Sivula K. Chem Comm. 2011; 47:8244–8246. [PubMed: 21706100]
38. Gomez ED, Barteau KP, Wang H, Toney MF, Loo YL. Chem Com. 2011; 47:436–438.
39. Kim HJ, Kim JW, Lee HH, Kim TM, Jang J, Kim JJ. J Phys Chem Let. 2011; 2:1710–1714.
40. Beaujuge PM, Frechet JMJ. J Am Chem Soc. 2011; 133:20009–20029. [PubMed: 21999757]
41. Li SS, Chang CP, Lin CC, Lin YY, Chang CH, Yang JR, Chu MW, Chen CW. J Am Chem Soc. 2011; 133:11614–11620. [PubMed: 21682313]
42. Liao HC, Tsao CS, Lin TH, Chuang CM, Chen CY, Jeng US, Su CH, Chen YF, Su WF. J Am Chem Soc. 2011; 133:13064–13073. [PubMed: 21755964]
43. Drain CM, Smeureanu G, Patel S, Gong X, Garno J, Arijeloye J. New J Chem. 2006; 30:1834–1843.
44. Drain, CM.; Smeareanu, G.; Patel, S. Dekker Encyclopedia of Nanoscience and Nanotechnology. Schwartz, JA.; Contescu, CI.; Putyera, K., editors. Marcel Dekker, Inc.; New York: 2004. p. 3481-3502.
45. Drain CM, Batteas JD, Flynn GW, Milic T, Chi N, Yablon DG, Sommers H. Proc Natl Acad Sci, USA. 2002; 99:6498–6502. [PubMed: 11880598]
46. Drain CM. Natl Acad Sci, USA. 2002; 99:5178–5182.
47. Bartelmess J, Ballesteros B, de la Torre G, Kiessling D, Campidelli S, Prato M, Torres T, Guldi DM. J Am Chem Soc. 2010; 132:16202–16211. [PubMed: 20973540]
48. Schlenker CW, Barlier VS, Chin SW, Whited MT, McAnally RE, Forrest SR, Thompson ME. Chem Mater. 2011; 23:4132–4140.
49. Kim JY, Bard AJ. Chem Phys Let. 2004; 383:11–15.
50. de la Torre G, Giacalone F, Segura JL, Martín N, Guldi DM. Chem Eur J. 2005; 11:1267–1280. [PubMed: 15635684]
51. Fukuzumi S, Ohkubo K, Imahori H, Shao J, Ou Z, Zheng G, Chen Y, Pandey RK, Fujitsuka M, Ito O, Kadish KM. J Am Chem Soc. 2001; 123:10676–10683. [PubMed: 11673999]
52. Quintiliani M, Kahnt A, Vazquez P, Guldi DM, Torres T. J Matr Chem. 2008; 18:1542–1546.
53. Brabec CJ, Gowrisanker S, Halls JJM, Laird D, Jia S, Williams SP. Adv Materials. 2010; 22:3839–3856.
54. Wang DH, Kim DY, Choi KW, Seo JH, Im SH, Park JH, Park OO, Heeger AJ. Chem Int Ed. 2011; 50:5519–5523.
55. Allen JE, Yager KG, Hlaing H, Nam CY, Ocko BM, Black CT. Appl Phys Lett. 2011; 99:163301–163303.
56. Hlaing H, Lu X, Hofmann T, Yager KG, Black CT, Ocko BM. ACS Nano. 2011; 5:7532–7538. [PubMed: 21838293]
57. Allen JE, Black CT. ACS Nano. 2011; 5:7986–7991. [PubMed: 21910410]
58. Wu WR, Jeng US, Su CJ, Wei KH, Su MS, Chiu MY, Chen CY, Su WB, Su CH, Su AC. ACS Nano. 2011; 5:6233–6243. [PubMed: 21749108]
59. Prato M, Maggini M, Giacometti C, Scorrano G, Sandona G, Farnia G. Tetrahedron. 1996; 52:5221–5234.
60. Bottari G, Suanzes JA, Trukhina O, Torres T. J Phys Chem Let. 2011; 2:905–913.
61. Rodríguez-Cordoba W, Noria R, Guarín CA, Peon J. Am Chem Soc. 2011; 133:4698–4701.

62. Troshin PA, Koeppe R, Peregudov AS, Peregudova SM, Egginger M, Lyubovskaya RN, Sariciftci NS. Chem Mater. 2007; 19:5363–5372.
63. Kaafarani BR. Chem Mater. 2010; 23:378–396.
64. Lee JK, Jang SI, Kim YG, Jang YW, Jeong BH, Kim JU, Jung KS, Kim MR. Molecular Crystals Liquid Crystals. 2008; 491:307–316.
65. Roussel O, Kestemont G, Tant J, De Halleux V, Aspe RG, Levin J, Remacle A, Gearba IR, Ivanov D, Lehmann M, Geerts Y. Molecular Crystals and Liquid Crystals. 2003; 396:35–39.
66. Hori T, Miyake Y, Yamasaki N, Yoshida H, Fujii A, Shimizu Y, Ozaki M. Appl Phys Express. 2010; 3:101602.
67. Sakamoto K, Ohno-Okumura E. Materials. 2009; 2:1127–1179.
68. Service RF. Science. 2011; 332:293. [PubMed: 21493832]
69. Hayashi H, Nihashi W, Umeyama T, Matano Y, Seki S, Shimizu Y, Imahori H. J Am Chem Soc. 2011; 133:10736–10739. [PubMed: 21699188]
70. Lei S, Yang Y, Zeng Q, Wang C. Langmuir. 2011; 27:3496–3501. [PubMed: 21341779]
71. Zhu F, Grobosch M, Treske U, Huang L, Chen W, Yang J, Yan D, Knupfer M. ACS Appl Mater Interfaces. 2011; 3:2195–2199. [PubMed: 21671615]
72. Placencia D, Wang W, Gantz J, Jenkins JL, Armstrong NR. J Phys Chem C. 2011; 115:18873–18884.
73. Bramble JP, Tate DJ, Revill DJ, Sheikh KH, Henderson JR, Liu F, Zeng X, Ungar G, Bushby RJ, Evans SD. Adv Func Mater. 2010; 20:914–920.
74. Laschat S, Baro A, Steinke N, Giesselmann F, Hägele C, Scalia G, Judele R, Kapatsina E, Sauer S, Schreivogel A, Tosoni M. Angew Chem Int Ed. 2007; 46:4832–4887.
75. Lux A, Rozenberg GG, Petritsch K, Moratti SC, Holmes AB, Friend RH. Synthetic Metals. 1999; 102:1527–1528.
76. Schmidt-Mende L, Fechtenkötter A, Müllen K, Moons E, Friend RH, MacKenzie JD. Science. 2001; 293:1119–1122. [PubMed: 11498585]
77. Milic T, Garno JC, Batteas JD, Smeureanu G, Drain CM. Langmuir. 2004; 20:3974–3983. [PubMed: 15969388]
78. Milic TN, Chi N, Yablon DG, Flynn GW, Batteas JD, Drain CM. Angew Chem Int Ed. 2002; 41:2117–2119.
79. Petritsch K, Dittmer JJ, Marseglia EA, Friend RH, Lux A, Rozenberg GG, Moratti SC, Holmes AB. Solar Energy Materials and Solar Cells. 2000; 61:63–72.
80. Gearba RI, Bondar AI, Goderis B, Bras W, Ivanov DA. Chem Mater. 2005; 17:2825–2832.

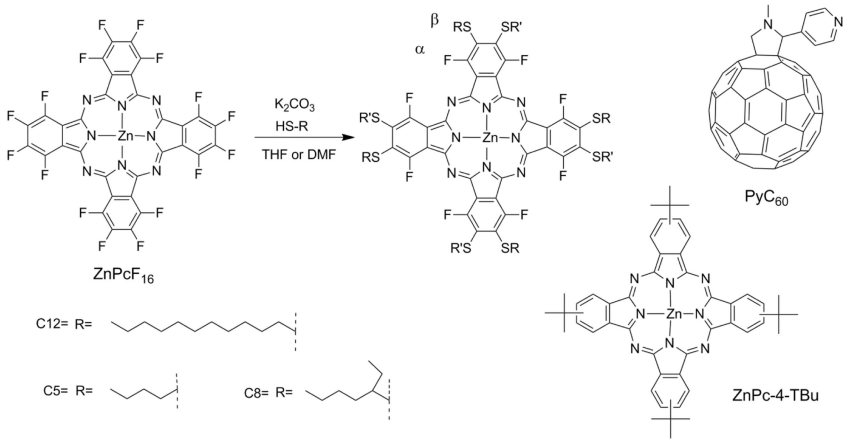

Figure 1.
Compounds used, see Table 1 for specific reaction conditions.

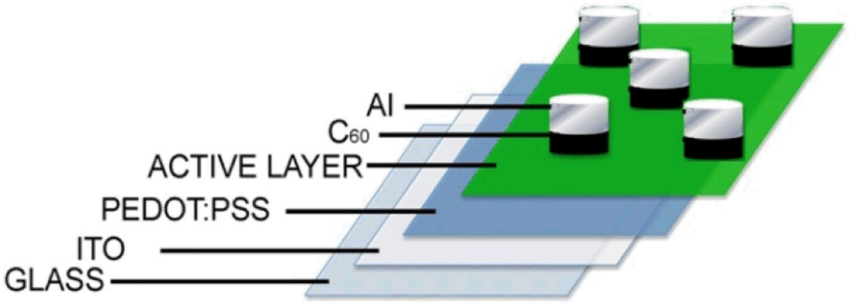

Figure 2.

A scheme of the device architecture; see abstract for picture. Samples for x-ray studies followed the same preparation excluding the C_{60} and Al electrodes. The evaporated C_{60} provides a better contact between the aluminum and active layer.

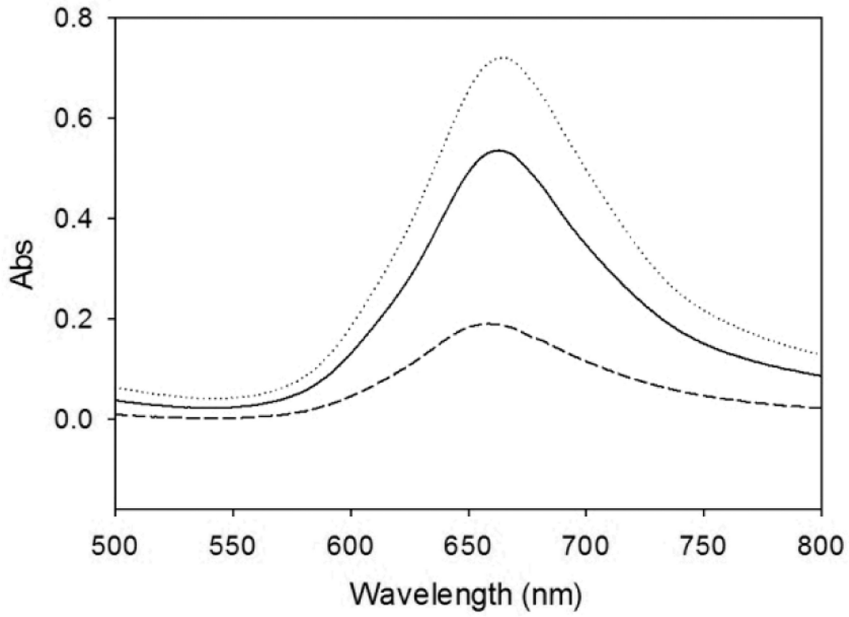

Figure 3.
UV-visible absorption spectrum of 70 nm films spin coated from equimolar solutions: ZnPc-4-C5 (dotted line); ZnPc-4-C8 (solid line); ZnPc-4-C12 (dashed line).

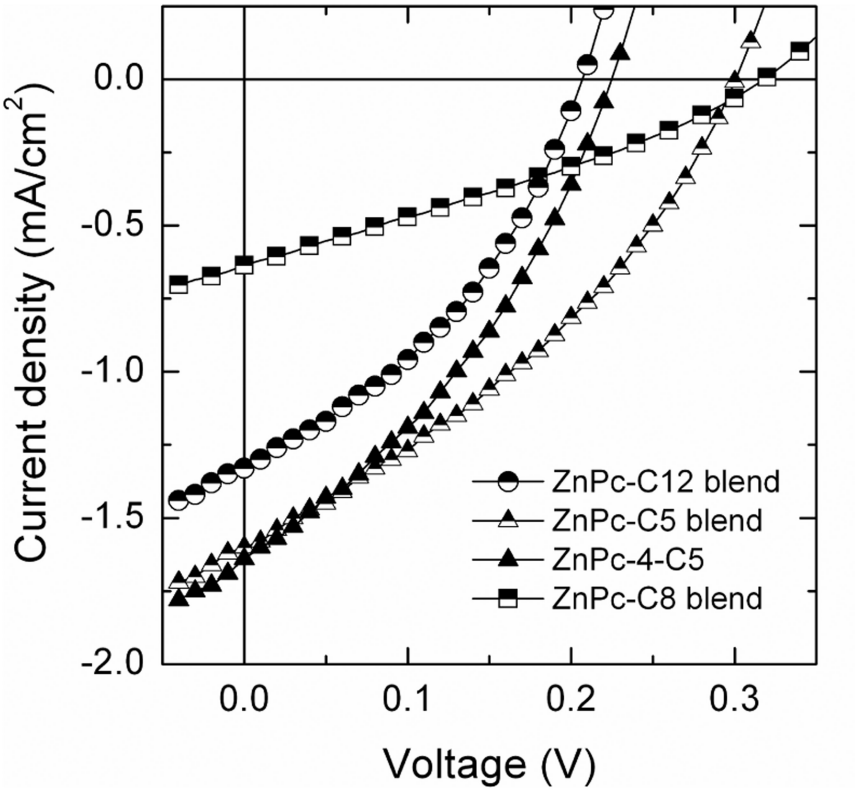

Figure 4.
Current-voltage characteristics of solar cells under 1 sun AM 1.5G conditions. All devices contain 30% (w/w) PyC_{60} unless otherwise stated.

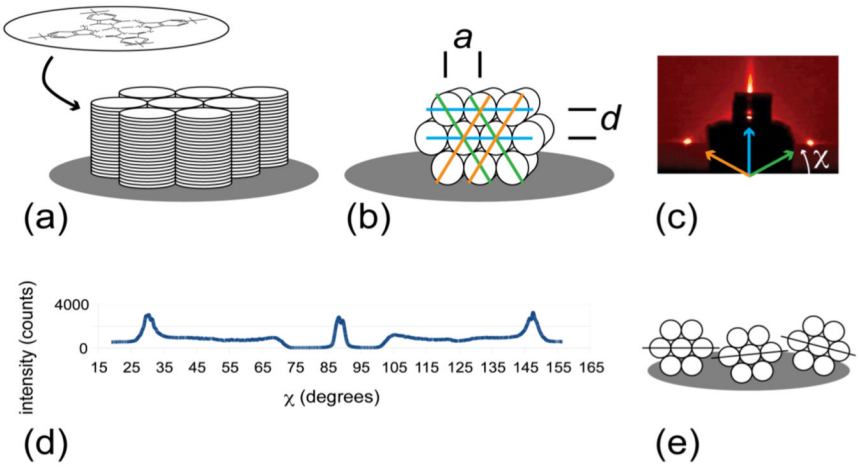

Figure 5.

(a) Homeotropically aligned columns of Pc molecules; (b) homogeneously aligned hexagonally packed columns, characterized by column spacing a and layer spacing d = a√3/2; (c) representative GISAXS pattern of ZnPc-8-C12 showing diffraction peaks from the six fold-symmetric column layer planes. The azimuthal angle χ is referenced from a horizontal axis; (d) x-ray intensity integrated through a small q range containing the Bragg peaks as a function of χ highlighting the 60° separation between peaks. Near χ =90°, flattened minima and irregular peak shape are due to transmission blocked by the beam stop; (e) depiction of variation in packed-column orientation which causes diffracted peaks to broaden in the χ direction.

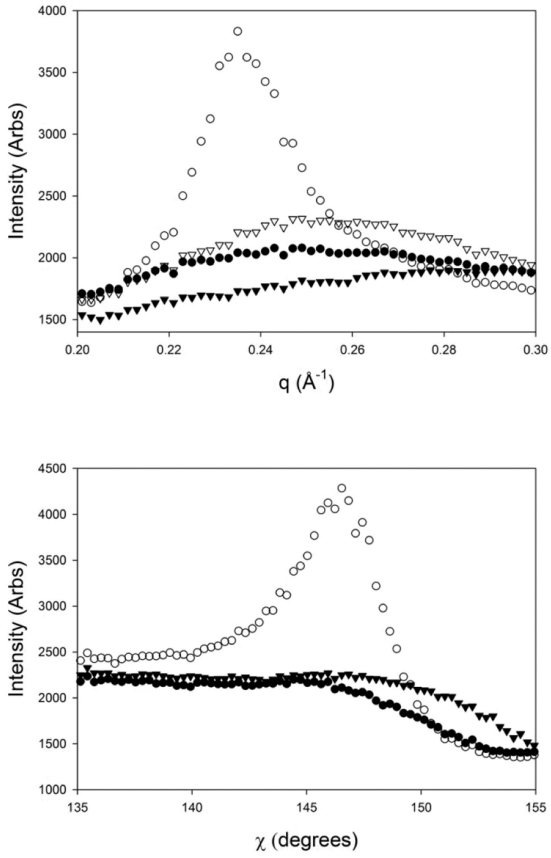

Figure 6.

Comparisonof GISAXS data for the alkylated ZnPc. ▼=ZnPc-4-TBu, •=ZnPc-4-C12, ○=ZnPc-8-C12, ∇= blend of ZnPc-4-C12: ZnPc-8-C12: ZnPc-4-TBu (17:66:17 by weight). Top: plots of intensity versus q in the region where diffraction spots corresponding to a hexagonal lattice appear. A diffraction ring is present in all samples except ZnPc-4-TBu. Bottom: plot of intensity versus χ.

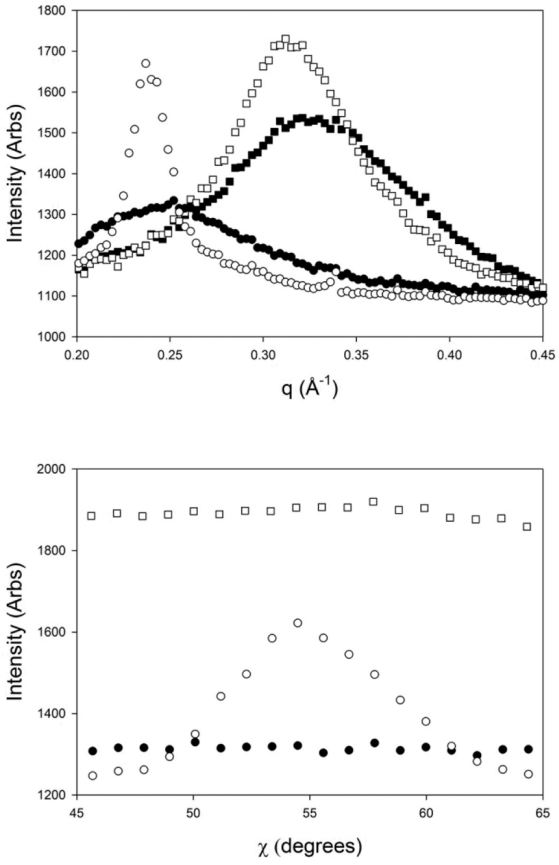

Figure 7.

Integrated GISAXS diffraction peak intensities for selected –C8 and –C12 films; ■=ZnPc-4-C8, □=ZnPc-8-C8, •=ZnPc-4-C12, ○=ZnPc-8-C12; Top: intensity versus q with χ integrated from 34.5-77.2; Bottom: Intensity versus χ with q integrated +/− 0.04 Å^{-1} about the center position determined from fits in the top panel. All films contain 30% PyC$_{60}$ by weight.

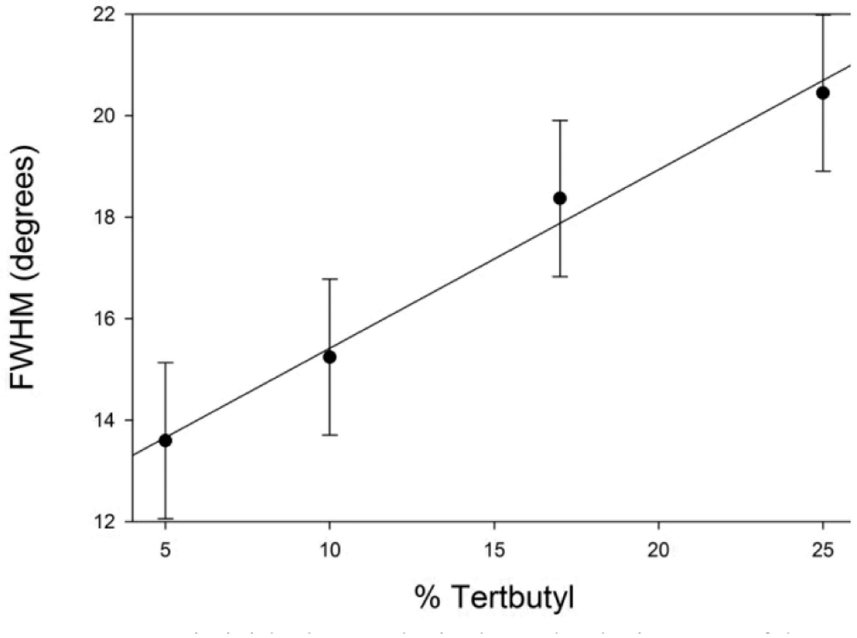

Figure 8.

Diminished LC order is shown by the increase of the FWHM of Gaussian fits to plots of the intensity versus χ integrated from q = 0 - 0.231 $Å^{-1}$ as the weight % of ZnPc-4-TBu increases in devices fabricated from 17:66 by weight blends of ZnPc-4-C12: ZnPc-8-C12.

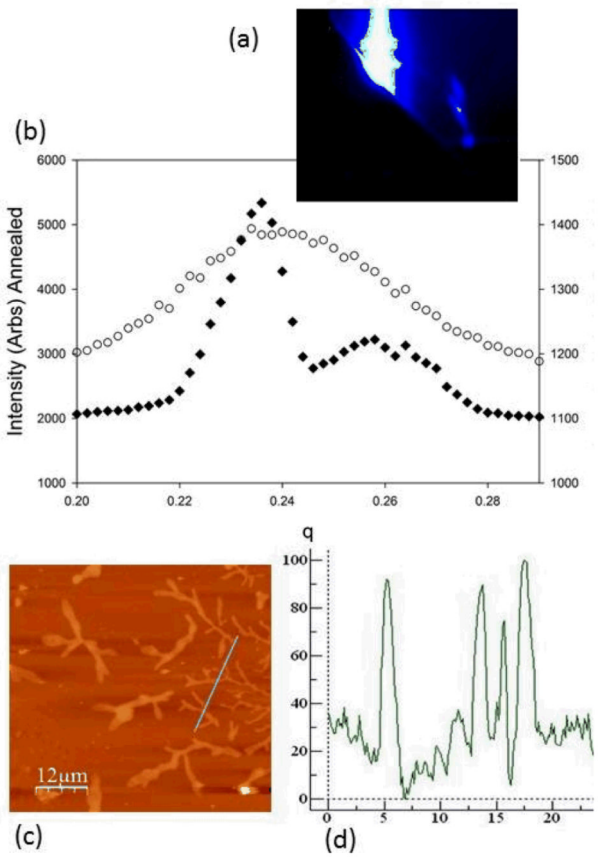

Figure 9.

(a) False color image of diffraction pattern of the ZnPc-8-C12 after annealing at 140°; (b) χ-integrated intensity versus q prior to (○) and following the anneal (◆), showing the segregation into two LC phases with distinct column layer spacings; (c) AFM height image of an annealed sample of ZnPc-8-C12 showing dendritic regions not observed prior to anneal; (d) AFM height trace along line indicated in (c).

Table 1

Compounds, reaction conditions, and strongest electronic absorption band. Use of the term “Pc-N-Cx Blend” where N is either 4 or 8and x is 12, 8, 5, or TBu, indicating the degree of substiution and alkane, respectively, ZnPc-4-TBu at 17:17:17 (w/w).

Compound[a]	Substituent[b]	# of thioalkanes	UV-visible λ_{max} (nm)	Reaction conditions[c]
ZnPc-4-C12 •	R or R'=1-dodecanethiol	4 – 6	708	K_2CO_3, stir 24 h at RT in THF
ZnPc-8-C12 ○	R=R'=1-dodecanethiol	8 – 10	736	K_2CO_3, stir 8 h in refluxing THF
ZnPc-4-C5 ▲	R or R'=1-pentanethiol	3 – 5	708	K_2CO_3, stir 2 h at 50 C in THF
ZnPc-8-C5 ▵	R=R'=1-pentanethiol	8 – 10	733	K_2CO_3, stir 3h in refluxing THF
ZnPc-4-C8 ■	R or R'=2-ethyl-1-hexanethiol	4 – 6	711	K_2CO_3, stir 24 h at 50 C in THF
ZnPc-8-C8 □	R=R'= 2-ethyl-1-hexanethiol	8 – 10	726	K_2CO_3, stir 2 h in refluxing DMF
ZnPc-4-TBu ▼	tert-butyl	4	680	Sigma-Aldrich

[a]The middle number indicates degree of substitution, the symbols are used in the GISAXS data plots.

[b]The major component; lesser amounts of other substitutionproducts are indicated in MALDI mass spectrometry and the range indicated in column 3.The α positions are substituted when there are >8 substiutions.

[c]All reaction used 100-fold excess thiol.

Table 2

PV cell parameters

	PCE%	Jsc mA cm^{-2}	Voc V	FF	Rs Ωcm^2
ZnPc-C12 blend	0.08	0.98	0.24	0.33	128
ZnPc-C5 blend	0.15	1.49	0.30	0.35	74
ZnPc-4-C5	0.12	1.43	0.25	0.35	76
ZnPc-C8 blend	0.06	0.64	0.31	0.30	281

Average of five devices, std error <10%, tested in open atmosphere